

Spatial and temporal variations in net primary production and long-term trends between 2003 and 2022 in the Indian Ocean: A synthesis using different models

V.V.S.S. Sarma^{1,2}, B. Sridevi¹, M.K. Ashitha¹

¹CSIR-National Institute of Oceanography, 176 Regional Centre, Visakhapatnam, India

²Academy of Scientific and Innovative Research (AcSIR), Ghaziabad, India

*Corresponding author (sarmav@nio.org)

Abstract

The measurements of net particulate primary production (NPP) with reference to space and time are limited in the Indian Ocean. Therefore, models are the only source of understanding spatial, temporal, and long-term variations. Different models have been developed to use remote sensing data to estimate NPP in the Indian Ocean. However, the accuracy of these models has not been evaluated. Here, we used the measured NPP data collected between 2003 and 2022 in the Indian Ocean to compare with different models such as Vertically Generalized Production (VGPM), Carbon-based Production (CbPM), Eppley-VGPM, and Carbon, Absorption, Fluorescence, Euphotic resolved (CAFE) models. This comparison suggested that CbPM simulated NPP with 10% underestimation compared to measured NPP in the Arabian Sea and South Indian Ocean (SIO), whereas VGPM simulated NPP well in the Bay of Bengal (BoB). The Eppley-VGPM over (under) estimated measured NPP by 20-30% in the SIO (Arabian Sea), while the CAFE model underestimated NPP in the BoB by 25%. No single model simulated the NPP well in the entire Indian Ocean compared to the measurements. All models reproduced seasonality in the Arabian Sea and SIO, but they failed in the case of the BoB. Compared to the measured NPP, the VGPM and CAFE models underestimated NPP, whereas the CbPM and Eppley-VGPM models overestimated it. Variable rates of changes in NPP in the past two decades were simulated in the Indian Ocean by different models. The long-term trends simulated by CbPM suggest decreasing trends in NPP south of 12°N and no trends north of 12°N in the Arabian Sea and increasing trends in NPP south of 20°S and decreasing trends north of 20°S in the SIO. The VGPM model indicated no significant trends in the BoB. The trends by the other models are variable and contrast in some regions. Therefore, the selection of an appropriate model to study long-term trends in NPP in the Indian Ocean is crucial.

Keywords: Primary production, remote sensing, models, comparison, long-term trends

Introduction

Marine primary production contributes approximately 50% of total global net primary production (NPP) with large spatial and temporal variations (Lurin, 1994; Longhurst et al., 1995; Field et al., 1998; Carr et al., 2006; Buitenhuis et al., 2013). The atmospheric carbon sequestered through the biological pump due to an increase in primary production offsets the flux of carbon due to enhanced vertical mixing of pCO₂-rich waters to the surface by upwelling (Mikaloff Fletcher et al., 2007; Gruber et al., 2009). The biological carbon pump is simulated to observe changes in response to global climate change, which alters the ocean's ability to store carbon and, therefore, impact atmospheric levels of CO₂ (Henson et al., 2011; Bopp et al., 2013; Boyd, 2015; Tagliabue et al., 2021).

The northern basin of the Indian Ocean, which consists of the Arabian Sea and the Bay of Bengal, is one of the highly productive regions in the global ocean due to the input of nutrients through coastal/offshore upwelling, winter convective mixing, river discharge and atmospheric deposition (Barber et al., 2001; Bhattathiri et al., 1996; Gauns et al., 2005; Dalabehera and Sarma, 2021; Sarma et al., 2022). Unlike the Pacific and Atlantic Oceans, equatorial upwelling does not occur in the Indian Ocean due to the presence of westerly winds (Schott et al., 2009), resulting in a flat thermocline (Murtugudde and Busalacchi, 1999; Xie et al., 2002). The South Indian Ocean (SIO) has low productivity due to oligotrophic conditions created by strong thermal stratification (Sarma and Dalabehera, 2019; Sarma et al., 2023). A significant amount of primary productivity data was collected, covering the entire Indian Ocean under the aegis of the International Indian Ocean Expedition (IIOE) in the early 1960s (Qasim, 1977; 1982). The measurement of primary productivity in the entire Indian Ocean was repeated under the aegis of the GEOTRACES program between 2012 and 2015 (Sarma and Dalabehera, 2019; Dalabehera and Sarma, 2021; Sarma et al., 2023). Seasonal primary production was measured under the aegis of the Joint Global Ocean Flux Study (JGOFS) in the Arabian Sea (Bhattathiri et al., 1996; Barber et al., 2001; Gauns et al., 2005) and the Bay of Bengal Processes Study (BoBPS) in the BoB (Gauns et al., 2005; Ramaiah et al., 2010). In addition to this, primary productivity in the northern Indian Ocean was measured in various national/international projects (Gomes et al., 2000; Satya Prakash et al., 2015; Rao and Sarma, 2022; Sarma et al., 2021; Sarma et al., 2018). Despite the collection of such data, the primary productivity measurements in the Indian Ocean were still limited in space and time. Unfortunately, there is no time-series observation station set up to examine how the Indian Ocean is responding to climate change with reference to marine primary production.

Several modelled primary production datasets are available to evaluate spatial, temporal, and long-term trends, such as the Vertically Generalized Primary Production model (VGPM; Behrenfeld and Falkowski, 1997), the Carbon-based Primary Production model (CbPM; Behrenfeld et al., 2005; Westberry et al., 2008), the Eppley-VGPM model, which is a modified version of VGPM by utilizing the exponential function of phytoplankton growth rates over a range of temperature proposed by Eppley (1972), and the CAFE model (Silsbe et al., 2016). The VGPM relies on the relationship between chlorophyll and temperature-derived growth rates, whereas the CbPM model relies on particulate backscattering estimates of phytoplankton carbon as a biomass indicator instead of chlorophyll. The CbPM approach allows for some of the variability in chlorophyll to be attributed to physiological adjustments to light and nutrients (e.g., photoacclimation), independent of changes in NPP. The more recent CAFE model (Silsbe et al., 2016) builds upon this approach by incorporating the influence of nonalgal absorption on the attenuation of the underwater light field. Several recent reports have suggested that primary production in the Indian Ocean is decreasing due to rapid warming. Roxy et al. (2015) reported a decrease in Chl-a off Somalia due to the weakening of upwelling (Roxy et al., 2015; D'Mello and Prasanna Kumar, 2018). A possible decrease in NPP in the future was projected by the year 2100 by different models in the Indian Ocean (e.g., Gregg and Rousseaux, 2019). Recently, Sridevi et al. (2023) reported a decline in NPP simulated by CbPM between the equator and 12oN in the northern Indian Ocean, and insignificant trends were observed to the north of 12oN. The lack of trends north of 12oN was attributed to the deposition of nutrients from atmospheric aerosol that may compensate for a decline in nutrient input through vertical mixing. Recently, Sarma et al. (2023) compared 12 hindcasts and two atmospheric inversion models in the Indian Ocean to examine their performance and best estimate CO₂ fluxes. It was noticed that none of these models performed well in the northern Indian Ocean, north of 18oS, due to weaker biological carbon pumps and physical mixing (Sarma et al., 2013; 2023). On the other hand, Sarma and Dalabehera (2019) compared limited measured primary production data collected during the intermonsoon period under the aegis of the GEOTRAES program with modelled NPP in the Indian Ocean and found that the CbPM model performed better along the cruise track.

Since the measured data do not cover the entire Indian Ocean and all months, it is difficult to evaluate possible changes in NPP due to climate change. Campbell et al. (2002) compared the performance of different models in the global ocean using measured NPP data. In this comparison, only data collected under the aegis of the USJGOFS program in the Arabian Sea were considered due to the unavailability of data from other regions. In the past two decades, the Indian Ocean has been enriched with more

NPP measurements under the aegis of more recent national and international programs, and so a more meaningful comparison is possible now. The objective of this study is to 1) compare NPP estimated by different models with measurements made between 2003 and 2022 due to the availability of continuous remote sensing data, 2) identify the best-performing NPP model in the Indian Ocean, and 3) derive long-term trends in NPP by different models in the Indian Ocean and identify the region where all models agreed. This information could help determine the most appropriate NPP model to compare with regional or global carbon cycle models for validation.

2. Material and methods

2.1. Methodology of different NPP models

Based on the remote sensing data, five models were proposed using variable parameters to derive NPP. A brief overview of each NPP model is given here. However, for the complete descriptions of the models, the reader is referred to the original publications. The Vertically Generalized Production Model (VGPM; Behrenfeld and Falkowski, 1997) is a Chlorophyll-based model that can be represented as:

$$NPP = 0.66125 * P_{opt}^b * (PAR/(PAR+4.1)) * Z_{eu} * Chl * D_{irr} \text{ --- (1)}$$

Where P_{opt}^b is the maximum chlorophyll-normalized primary production in the water column ($mgC(mgChl)^{-1} h^{-1}$), PAR is photosynthetic active radiation at the surface ($mol\ photon\ m^{-2}$), Z_{eu} is the euphotic depth defined as the depth of 1% of surface PAR reaches, Chl is the concentration of chlorophyll-a ($mg\ m^{-3}$) and D_{irr} is the day length time in hours. The polynomial equation was developed by relating P_{opt}^b with SST.

The Carbon-based Production Model (CbPM; Westberry et al., 2008) is based on the phytoplankton physiology. Phytoplankton respond to changes in light, nutrients, and temperature and modify their cellular pigment concentrations. These changes are reflected in the Chl: C ratio (e.g., Geider, 1987; Sakshaug et al., 1989; MacIntyre et al., 2002). The particulate beam attenuation coefficient at 660 nm covaries with the particulate organic carbon concentration (e.g., Bishop et al., 1999; Claustre et al., 1999). Therefore, the Chl: C ratio from the remote sensing is considered in the CbPM to assess phytoplankton physiology and estimate NPP using the following equation:

$$NPP = C_{phyto}(z) * \mu(z) * dz \text{ ---- (2)}$$

In this model, NPP is a product of phytoplankton biomass in terms of carbon ($mgC\ m^{-3}$) and its growth rate (μ, d^{-1}) integrated over the photic zone. The phytoplankton growth rate is estimated from the relationship between laboratory-based measurements of Chl : C and a light dependence.

The Carbon, Absorption, Fluorescence, Euphotic-resolving NPP model (CAFÉ; Silsbe et al., 2016) is an absorption-based model, and NPP is estimated as:

$$\text{NPP} = E_o(\lambda, z) * a_{ph}(\lambda, z) d\lambda * \Phi_{\mu}(z) dz \text{ ----- (3)}$$

Where $E_o(\lambda, z)$ is the spectral, scalar irradiance, $a_{ph}(\lambda, z)$ is the spectral phytoplankton absorption coefficient, and Φ_{μ} is the light-dependent quantum yield of carbon fixation, which is derived similarly to the P-I curve. These are integrated over the photic zone.

The Eppley-VGPM-NPP model is a Chlorophyll-based model and has the same structure as the VGPM (Behrenfeld and Falkowski, 1997) but uses the exponential relationship of P^b_{opt} with SST by Morel (1991) and the temperature-dependent growth function of Eppley (1972). In this model, NPP varies predictably with chlorophyll concentration. The NPP by Eppley-VGPM can be written as:

$$\text{NPP} = \text{Chl} * P^b_{opt} * \text{day length} * [0.66125 * \text{PAR} / (\text{PAR} + 4.1)] * Z_{eu} \text{ ----- (4)}$$

The P^b_{opt} is derived using the exponential function following Eppley (1972).

$$P^b_{opt} = 1.54 * 10^{[(0.0275 * \text{SST}) - 0.07]} \text{ ---- (5)}$$

2.2. Data used

The main objective of this study is to evaluate how different primary productivity models perform with reference to the measured rates. In-vitro primary productivity measurements carried out in the Indian Ocean between 2003 and 2022 were used for this analysis. The photic zone integrated phytoplankton biomass (as Chlorophyll-a (Chl-a)) and net community particulate primary production (NPP) were considered in this study. The phytoplankton biomass normalised NPP, called P_b , was computed by dividing the photic zone integrated NPP with Chl-a to evaluate the efficiency of the phytoplankton in fixing the carbon. The concentration of chlorophyll-a was measured by filtering 3 to 5 litres of the sample through a GF/F filter (0.7 μm , 47 mm, Whatman) and pigment retained on the filter was extracted into 90% acetone and fluorescence of the extract was measured using a spectrofluorometer. The water samples from 7 to 8 depths (typically 0, 10, 20, 30, 50, 75, 100, and 120m) were collected into 1 L transparent Nalgene bottles and incubated onboard the research vessel in the incubator for NPP measurements covering the light depth ranges between 100% (surface) and the depth where 1% of surface photosynthetic active radiation (PAR) reaches and deep chlorophyll maxima (DCM). Each sample was spiked with 1 ml of $\text{NaH}^{14}\text{CO}_3$ (5 $\mu\text{Ci ml}^{-1}$, Department of Atomic Energy, India) or 0.2 ml of 2mM $\text{NaH}^{13}\text{CO}_3$ (99 atomic percentage; Sigma Aldrich, USA) and incubated in the incubator on deck. The samples that used ^{13}C or ^{14}C spike are given in Table 1. At each depth, three light and two dark bottles were incubated. The incubator temperature was maintained close to the in-situ

temperature. Neutral density screens were used to simulate light levels with depth. The incubation was conducted for 24 hours. After the incubation, samples were filtered through pre-combusted (at 300°C for six hours) glass fibre (GF/F) filters (pore size of 0.7 µm) under gentle suction, and filters were stored at -20°C until analysis. The exudation of DOC was not measured in these experiments. According to Hama et al. (1983), the NPP measured using a ¹³C tracer is almost equivalent to the ¹⁴C tracer method. The detailed method of incubation conducted and conditions maintained can be found in the literature (Barber et al., 2001; Sarma and Dalabehera, 2019; Dalabehera and Sarma, 2021). The depth-based primary productivity and Chl-a measurements were integrated over the photic depth using the trapezoidal method.

The monthly mean photic zone integrated primary productivity data from different models such as VGPM, CbPM, Eppley-VGPM model and CAFE models were obtained from www.orca.science.oregonstate.edu. All models used Chlorophyll-a, PAR and sea surface temperature (SST) as input parameters from MODIS. In addition, the diffuse attenuation coefficient at 490 from MODIS and mixed layer depth from the HYCOM (Chassignet et al., 2007) were used in the CbPM and CAFE models, whereas the depth of nitracline that was used in the CbPM model, and sea surface salinity that was used in the CAFE model was taken from World Ocean Atlas (Conkright et al., 2002). All the required parameters to estimate NPP using different models were not always available on the day of measurements due to cloud conditions. Therefore, remote sensing data collected within 3 to 7 days of the measurement date were used to compute NPP by different models. Therefore, some uncertainty may be anticipated.

2.3. Deriving long-term trends

The long-term trends with reference to seasons were analyzed using a linear trend analysis for NPP. The NPP data from various models were averaged for different seasons, such as winter (December, January and February), spring (March, April and May), Summer (June, July and August) and Fall (October and November).

2.4. Statistical analysis

To compare the in situ measured (x_i) and modelled NPP (y_i) data, a statistical analysis was conducted. The slope and intercept (I) of the linear regression and correlation coefficient (R) and coefficient of determination (R^2) were computed. The log difference errors between measured and modelled NPP ratio (r) were computed as $1/N \sum x_i/y_i$, where N is the number of match-up points. The \log_{10} RMSE was

computed as the square root of $(\log_{10}(x_i) - \log_{10}(y_i))^2/N$. The geometric mean and one-sigma range of the ratio $F = \text{value}_{\text{modeled}}/\text{value}_{\text{mean}}$

are given by F_{med} , F_{min} , and F_{max} , respectively. The values closer to 1 are more accurate than those deviating from 1. UPD is the unbiased percentage difference, and it is estimated as $1/N \sum (x_i - y_i)/(x_i + y_i)/2$. The statistical analysis was performed following Campbell et al. (2002). The Matlab tool was used to conduct the statistical analysis.

3. Results and Discussion

3.1. Possible biases in measured NPP data in the Indian Ocean

The measured NPP data between 2003 and 2022 were used in this study as the remote sensing NPP data from MODIS are available during this period. A significant amount of NPP data has been collected with reference to space and time in the northwestern Arabian Sea (AS) and the northeastern Bay of Bengal (BoB) in the Indian Ocean (Fig. 1a,b). In contrast, the spatial and temporal coverage in NPP measurements in the SIO remains poor (Fig. 1c). For instance, NPP data were collected from January to April, July, September, October and December in the Arabian Sea, and all months except January, May and November in the BoB (Fig. 1a,b). In the case of SIO, NPP was measured only from February to June and October to November (Fig. 1c). Therefore, some bias may be anticipated, especially in the SIO, due to a lack of seasonal coverage.

3.2. Spatial and temporal variability in measured NPP in the Indian Ocean

The available measured Chl-a, NPP and P^b data, irrespective of the time of data collection, was integrated over the photic zone and averaged for each sub-basin of the tropical Indian Ocean is plotted in Figure 2 to examine its spatial variability. The measured photic zone integrated Chl-a was higher in the SIO ($68 \pm 59 \text{ mg m}^{-2}$), followed by BoB ($19.5 \pm 13 \text{ mg m}^{-2}$) and Arabian Sea ($19.2 \pm 56 \text{ mg m}^{-2}$) with large variations in the SIO as indicated by the high standard deviation (Fig. 2a). Insignificant differences in photic zone integrated Chl-a were observed between the Arabian Sea and the BoB. In the case of measured NPP, it was higher in the Arabian Sea ($981 \pm 55 \text{ mgC m}^{-2} \text{ d}^{-1}$), followed by BoB ($565 \pm 418 \text{ mgC m}^{-2} \text{ d}^{-1}$) and SIO ($443 \pm 308 \text{ mgC m}^{-2} \text{ d}^{-1}$), which is in contrast to that of Chl-a (Fig. 2a). However, the standard deviation is high, especially in the SIO, BoB and EIO, which may reflect high bias in the measurements,

potentially due to a higher frequency of measurements during bloom periods. The spatial variation in Chl-a followed the nutrient concentrations in the surface (WOA 23; Reagan et al., 2023; Supplementary Figure S1), with higher concentrations of nutrients in the Arabian Sea due to seasonal upwelling and convective mixing (De Souza et al., 1996; Madhupratap et al. 1996; Morrison et al., 1998) compared to other regions of the Indian Ocean. Nutrient availability mainly controls the rate of NPP rather than light in the tropical Indian Ocean (Barber et al., 2001; Sarma and Dalabehera, 2019; Dalabehera and Sarma, 2021; Sarma et al., 2023). Enhanced NPP in cyclonic eddies (Prasanna Kumar et al., 2004; Sarma et al., 2018), cyclone-influenced regions (e.g., Maneesha et al., 2011) and coastal upwelling regions (Barber et al., 2001) have been reported due to the availability of nutrients. Lower NPP in the BoB relative to the Arabian Sea was attributed to strong salinity stratification that limits the vertical mixing (Gauns et al., 2005) and nutrient supply to the photic zone (Sarma et al., 2013). The lowest NPP was observed in the SIO due to the prevalence of oligotrophic conditions caused by strong thermal stratification (Satya Prakash et al., 2015; Sarma and Dalabehera, 2019; Dalabehera and Sarma, 2021; Sarma et al., 2023).

Higher P^b was observed in the Arabian Sea (32 ± 29 mgC mg Chl-a⁻¹ d⁻¹), and it decreased towards the SIO to <5 mgC mg Chl-a⁻¹ d⁻¹, suggesting that the phytoplankton efficiency to fix atmospheric carbon dioxide decreases from north to south in the Indian Ocean (Fig. 2c). The lower P^b in the SIO may also be caused by nutrients, seasonal light and trace metal limitations (Satya Prakash et al., 2015), whereas higher P^b in the Arabian Sea is associated with high nutrient inputs.

3.3. Comparison of measured NPP with different models in the Indian Ocean

The measured NPP data, plotted irrespective of season in Figure 3a, reveals the highest mean NPP in the Arabian Sea and the lowest in the SIO. In the following subsections, the NPP estimated using the different models is compared with the measured NPP. This comparison reveals how well the different NPP models capture the measured NPP in the Indian Ocean.

3.3.1. Vertically Generalized Production Model (VGPM)

Compared to the measured NPP, the VGPM model failed to reproduce the spatial variability in the NPP in the Indian Ocean. For instance, measured NPP indicates higher production in the Arabian Sea compared to the BoB, however, the VGPM model displays a weak difference between these two basins (Fig. 3b). The coefficient of determination between the measured and VGPM-simulated NPP was weak ($R^2=0.28$) compared to the other models, with the

highest UPD (37%) in the Arabian Sea. Fmed suggests that VGPM is overestimating NPP by 46% compared to measured NPP in the Arabian Sea (Table 3). Similarly, VGPM did not perform well in the SIO, where an insignificant coefficient of determination ($R^2=0.08$), high logRMSE (0.10), and high UPD (29.3%) were observed. In the SIO, the VGPM model overestimates NPP by 38% compared to measured NPP (Table 3). In contrast, a significant coefficient of determination ($R^2=0.54$), low logRMSE (0.01) and UPD (~8%) were observed in the BoB (Table 3). The VGPM model underestimates the measured NPP by only 8% in the BoB, suggesting that VGPM is performing better in the BoB than other basins in the Indian Ocean.

Since the parameterization of the VGPM is based on the surface values, it may not be able to capture the increase in NPP due to physical processes, as evidenced by low NPP off Oman and Somalia coasts where intense upwelling and mixing occurs. In contrast, the VGPM performed well in the BoB, which has a stratified water column, shallow photic depth and low Chl-a, and most of the NPP occurs in the upper ocean that can be captured by the surface measurements.

3.3.2. Carbon-based Production Model (CbPM)

The CbPM model captured the spatial variability in NPP in the tropical Indian Ocean better compared to VGPM and displayed higher NPP in the Arabian Sea, followed by the BoB and SIO. In contrast, the CbPM model simulated higher NPP in the BoB than the measured NPP (Fig. 3c) whereas the CbPM-simulated NPP in the Arabian Sea is close to the measured values. The inaccurate simulation of CbPM in the BoB may arise from the Chl-a: C ratio used in this model. The BoB receives a significant fraction of the terrestrial particulate organic carbon (POC) from rivers with large spatial variability (Sherin et al., 2018; Sarma et al., 2019; Kurian et al., 2023). The modification of measured Chl-a: C ratios may improve the performance of CbPM in the BoB. The statistical analysis shows that the coefficient of determination of NPP between measured and CbPM-simulated was lower in the BoB ($R^2=0.42$) compared to VGPM and higher logRMSE (0.10) and UPD (60.7%) compared to VGPM (Table 3). The CbPM model underestimates NPP in the BoB by nearly 50% (Table 3). In contrast, the coefficient of determination in the Arabian Sea ($R^2=0.74$) and SIO ($R^2=0.24$) had low UPD of 23 and 2.6%, respectively. The NPP simulated by CbPM seems to be underestimating the measurements by only ~10% in the Arabian Sea and SIO, suggesting this model is performing well in these two basins.

3.3.3. Eppley-VGPM

The spatial trends in NPP simulated by the Eppley-VGPM model are comparable to that of the CbPM model. The NPP in the SIO was well reproduced by the Eppley-VGPM model compared to VGPM and CbPM, especially south of 30°S (Fig. 3d). In contrast, Eppley's growth function overestimated NPP in the BoB. The coefficient of determination between measured and Eppley-VGPM NPP was low in the Arabian Sea ($R^2=0.30$) and SIO ($R^2=0.32$) compared to the BoB ($R^2=0.52$). Among the three basins of the Indian Ocean, the lowest UPD was observed in the SIO (~16%), compared to the Arabian Sea (~33%) and the BoB (71%). The Eppley-VGPM model overestimates measured NPP by 18% in the SIO, whereas it overestimates by ~50% in the BoB and underestimates by 30% in the Arabian Sea (Table 3). The statistical analysis suggests that the Eppley-VGPM model is performing well in the SIO compared to other sub-basins in the Indian Ocean.

3.3.4. CAFE model

This model did not display significant spatial variability compared to measured NPP (Fig. 3e). Among other models, the performance of CAFE is the weakest, especially in reproducing spatial variations in NPP. The coefficient of determination in the BoB is insignificant ($R^2=0.0$) compared to the Arabian Sea ($R^2=0.34$) and SIO ($R^2=0.38$). The UPD in all sub-regions of the Indian Ocean were >20%. The CAFE model overestimates measured NPP by ~30% in the Arabian Sea while underestimating by ~25% in the BoB and the SIO (Table 3).

The weak performance of the CAFE model may be due to the unique optical characteristics of the Indian Ocean, as it is influenced by river runoff that brings a significant amount of suspended load that alters the light absorption and backscatter.

Among the different NPP models, CbPM performs well in the Arabian Sea and SIO with underestimation by 10% compared to measurements, whereas VGPM performs well in the BoB (Fig. 3).

3.4. Comparison of spatial variability and annual mean NPP by different models measured in the Indian Ocean

To examine how different models reproduced basin mean NPP, the climatological mean of NPP generated by the different models was compared (Fig. 4) with measured mean NPP in different regions in the Indian Ocean.

3.4.1. Arabian Sea

All models, except CAFE, displayed high NPP ($>900 \text{ mgC m}^{-2} \text{ d}^{-1}$) along the coasts of Somalia, Oman and Indian coasts in the northern Indian Ocean, however, the extent of high NPP regions are different (Fig. 4a-d). For instance, the CAFE model shows relatively higher NPP off the Oman and Somalia coasts ($\sim 700 \text{ mgC m}^{-2} \text{ d}^{-1}$), but it was the lowest compared to other models in this region (Fig. 4d). The VGPM model shows a high NPP of $>900 \text{ mgC m}^{-2} \text{ d}^{-1}$ off the Oman coast that spreads up to 100-150 km offshore (Fig. 4a). In contrast, the CbPM and Eppley-VGPM models displayed higher NPP ($>900 \text{ mgC m}^{-2} \text{ d}^{-1}$) in the entire Arabian Sea, north of 10°N (Fig. 4b,c). The high NPP off Somalia was restricted close to the coast in the VGPM model (Fig. 4a), whereas it spread up to 200 km from the coast in other models (Fig. 4b-c). The NPP along the Indian coast was the lowest in the CAFE model, followed by VGPM, compared to the other models. Overall, the CAFE and VGPM models simulated lower NPP in the entire Arabian Sea compared to the other models. The annual mean measured NPP for the entire Arabian Sea (north of 10°N) was $960 \pm 539 \text{ mgC m}^{-2} \text{ d}^{-1}$, which was close to the values simulated by the CbPM ($1035 \pm 358 \text{ mgC m}^{-2} \text{ d}^{-1}$) and Eppley-VGPM ($1054 \pm 364 \text{ mgC m}^{-2} \text{ d}^{-1}$) models, whereas the CAFE and VGPM models underestimated NPP ($\sim 500 \text{ mgC m}^{-2} \text{ d}^{-1}$), due to weaker simulations in the coastal upwelling regions in the Arabian Sea (Fig. 4a). The measured mean NPP falls within the modelled NPP during different months (Fig. 4a).

3.4.2. Bay of Bengal

The BoB is reported to be a less productive region compared to the Arabian Sea due to strong stratification (Gauns et al., 2005). The VGPM and CAFE models simulated lower NPP compared to other models and also compared to the measured NPP in the BoB (Fig. 5b). The VGPM model simulated increases in NPP at the Ganges/Brahmaputra outflow region and close to the coast along the east coast of India, Burma and Thailand, but this was absent in the CAFE model (Fig. 4a,d). In contrast, the CbPM, and Eppley-VGPM models estimated higher NPP in the BoB with values almost equivalent NPP in the Arabian Sea along the coastal region ($>900 \text{ mgC m}^{-2} \text{ d}^{-1}$) and offshore regions ($>700 \text{ mgC m}^{-2} \text{ d}^{-1}$) (Fig. 4). Lower NPP ($400\text{-}500 \text{ mgC m}^{-2} \text{ d}^{-1}$) was simulated by the VGPM and CAFE models compared to the measurements, whereas the other models simulated higher NPP ($750 \text{ to } 1000 \text{ mgC m}^{-2} \text{ d}^{-1}$). The annual mean measured NPP in the Bay of Bengal was $395 \pm 185 \text{ mgC m}^{-2} \text{ d}^{-1}$, which was close to the VGPM ($452 \pm 188 \text{ mgC m}^{-2} \text{ d}^{-1}$) and CAFE ($470 \pm 144 \text{ mgC m}^{-2} \text{ d}^{-1}$) simulated values (Fig. 6b). In contrast, the CbPM and Eppley-VGPM and models generated

much higher NPP values ($>800 \text{ mgC m}^{-2} \text{ d}^{-1}$). The VGPM and CAFE models did not perform well in the Arabian Sea, where upwelling and convective mixing are important. In contrast, the simulations of VGPM and CAFE are close to those measured in the BoB, where strong stratification and weaker mixing occur (Fig. 6b). The VGPM model is parameterized with reference to SST and Chl-a. In contrast, the CAFE model uses several parameters, including mixed layer depth (Table 2). Regardless, both models underestimate NPP in upwelling and well-mixed regions like the Arabian Sea.

3.4.3. South Indian Ocean

The measured NPP in the SIO displayed significant meridional variability with moderate NPP between 10 and 30°S , higher NPP between 35 and 45°S and the lowest NPP south of 45°S . The highest NPP was simulated in the entire SIO by the CAFE model and the lowest by the VGPM model (Fig. 4a,d). The highest NPP in the mode water region, between 35 and 45°S , was simulated by the CAFE model and the lowest was simulated by the VGPM model. The lowest NPP was simulated south of 45°S in the Eppley-VGPM and VGPM models, whereas the highest was simulated by the CAFE model, followed by CbPM. The annual mean NPP in the SIO simulated by the VGPM ($310 \pm 231 \text{ mgC m}^{-2} \text{ d}^{-1}$), CbPM ($353 \pm 194 \text{ mgC m}^{-2} \text{ d}^{-1}$) and CAFE ($377 \pm 99 \text{ mgC m}^{-2} \text{ d}^{-1}$) models were close to the mean measured NPP of $377 \pm 321 \text{ mgC m}^{-2} \text{ d}^{-1}$ whereas the Eppley-VGPM model underestimated NPP ($233 \pm 135 \text{ mgC m}^{-2} \text{ d}^{-1}$; Fig. 5c).

3.5. Comparison of monthly mean NPP by different models

To examine the simulations of seasonality in NPP in different basins, the monthly mean NPP by different models were compared.

3.5.1. Arabian Sea

All models displayed typical bi-modal distribution with higher NPP during summer (June to September) and winter (December to February) compared to spring intermonsoon (March to June). Among the models, the peak in NPP during summer was weaker in the CAFE model compared to the other models (Fig. 6a). Barber et al. (2001) reported the occurrence of the peak in NPP during summer (July-August) in the Arabian Sea, associated with the input of nutrients through upwelling. This seasonality was missing in the CAFE model, which showed an insignificant difference in NPP between winter and spring (Fig. 6a) in the Arabian Sea. The highest monthly mean NPP in the Arabian Sea was simulated by the Eppley-VGPM model, followed by CbPM, whereas the VGPM model simulated the lowest values (Fig. 6a). The measured monthly mean NPP in the Arabian Sea fell among model

simulated values, but with relatively higher rates during January, July and September compared to modelled values (Fig. 6a).

3.5.2. Bay of Bengal

Unlike the Arabian Sea, the weak seasonal variability in measured NPP was simulated in the BoB by all models due to a lack of seasonal convective mixing and strong upwelling caused by freshwater stratification (Fig. 6b). The CbPM and Eppley-VGPM model-simulated NPP rates were almost double that of the VGPM and CAFE models. The CbPM and Eppley-VGPM models displayed similar and high NPP from January to March and November to December, whereas NPP simulated by the CbPM model was lower than Eppley-VGPM during other months. Gauns et al. (2005) reported significant seasonal variations with higher NPP during winter and the lowest during summer in the Bay, which was attributed to low light (Gomes et al., 2000) due to river discharge that delivers a high suspended load. None of the models were able to reproduce the seasonality seen in the BoB (Fig. 6b).

3.5.3. South Indian Ocean

The seasonality in NPP was the lowest from June to September and the highest from November to March in the SIO. Unlike in the Arabian Sea, the highest NPP was estimated by the CAFE, CbPM and VGPM models, and the lowest was estimated by the Eppley-VGPM model in the BoB during all months. The measured NPP was close to that of the modelled NPP during February, March and October.

Overall, seasonality in the NPP was well reproduced by all models in the Arabian Sea and SIO, but the models failed to do so in the BoB. The VGPM model showed relatively lower NPP in all basins, except in the SIO. The CbPM and Eppley-VGPM models generated the highest NPP in the Indian Ocean with large variability in space.

3.6. Long-term changes in the NPP by different models.

To examine the long-term variability in the NPP, the trends were derived between 2003 and 2022 by the different models and the spatial variability in trends of NPP (Fig. 7) are discussed below in different sub-basins of the Indian Ocean.

3.6.1. Arabian Sea

The long-term NPP trends simulated by different NPP models are not uniform in the Arabian Sea. Based on the comparison between measured and modelled NPP, the CbPM model seems to be performing well in the Arabian Sea. The long-term NPP trends simulated by the CbPM model suggest decreasing trends in NPP south of 12°N in the Arabian Sea during all seasons with some spatial

variability (Fig. 7e-h), and no trends were simulated north of 12°N during all seasons except in fall when a decline in NPP was observed. A significant increase in NPP was simulated off Oman's coast during summer by the CbPM model (Fig. 7g). These weak NPP trends are consistent with studies that have revealed that nutrient input through vertical mixing has decreased in the recent decades due to warming of the upper ocean, however, the decline in nutrient input has been compensated by increased deposition of nutrients from the atmosphere, resulting in a lack of significant trends in the NPP in the Arabian Sea (Tandule et al., 2022; Sridevi et al., 2023; Malsang et al., 2024).

In contrast, the VGPM model suggests no significant trends in the entire Arabian Sea during winter and fall, and an increase (decrease) in NPP off Oman during spring (summer) (Fig. 7b,c). The Eppley-VGPM model indicates an increase in NPP off Oman during winter and spring (Fig. 7i,j), with insignificant trends in other seasons. The CAFE model showed a decline in NPP in the recent decades in the entire Arabian Sea, except in the northern Arabian Sea during winter (Fig. 7m-p). Since the Eppley-VGPM and CAFE models underestimated measured NPP by >30%, the trends derived by them may not be accurate in the Arabian Sea.

3.6.2. Bay of Bengal

In the case of the BoB, the VGPM model-simulated NPP is comparable to the measured NPP with an underestimation of 8%. Both the VGPM and the Eppley-VGPM models did not show any significant trends in NPP in the BoB during the past two decades, which is consistent with the aforementioned studies suggesting compensation of a decline in nutrient input through vertical mixing by increased atmospheric deposition. In contrast, the CbPM and CAFE models significantly underestimated NPP and generated declining trends during all seasons in the BoB. Therefore, the Eppley-VGPM simulations of weaker or no trends in the NPP may be more accurate.

3.6.3. South Indian Ocean

The CbPM model simulated increasing trends in NPP south of 20°S and decreasing trends north of 20°S in the SIO (Fig. 7e-h). In contrast, the Eppley-VGPM model simulated increasing trends in NPP south of 20°S during boreal winter and no significant trends during other seasons. The CAFE model generated increasing trends in NPP south of 30°S during boreal spring and summer and no trends during other seasons. Since the simulation of the CbPM model was close to the measured NPP, the increase in NPP, though patchy, south of

20°S, and the decline north of 20°S in the SIO generated by this model may represent real trends.

4. Summary and Conclusions

Using the measured NPP data collected between 2003 and 2022, the NPP estimated by different models were compared in the Indian Ocean. This comparison shows that the CbPM simulated NPP is close to the measured NPP in the Arabian Sea and SIO with 10% underestimation. In contrast, NPP simulated by the VGPM model reproduced measured NPP values reasonably well in the BoB. The CAFÉ (Eppley-VGPM) models simulated NPP reasonably well in the SIO with under (over) estimation by 24% (18%). Similarly, the CAFE model simulated NPP relatively well in the BoB after VGPM, with an underestimation of 25%. This study suggests that none of the models were able to simulate NPP well in the entire Indian Ocean. The VGPM model showed relatively lower NPP in all basins, except in the SIO, whereas the CbPM and Eppley-VGPM models displayed higher NPP in all basins. Therefore, the selection of the NPP model is crucial for the simulation of NPP in various sub-regions of the Indian Ocean.

With reference to the long-term trends in NPP, the CbPM model suggests decreasing trends in NPP south of 12°N and no trends north of 12°N in the Arabian Sea during all seasons with spatial variability. In contrast, the CbPM model simulated increasing trends in NPP south of 20°S and decreasing trends north of 20°S in the SIO. The VGPM model did not show any significant trends in NPP in the BoB. The long-term trends simulated by the models are different and sometimes contrasting; therefore, caution is warranted in choosing the NPP model for interpreting the role of climate change in influencing long-term NPP trends in the Indian Ocean. The trends simulated by the models that have significant agreement with the measured NPP may be more accurate. However, it is not clear how these models capture long-term trends due to a lack of validation data. This comparison exercise should be continued in the future once new data have become available from the Indian Ocean for validation.

Acknowledgements

We would like to thank Drs. Sanjeev Kumar, Aravind Singh, and N.V. Madhu for providing their published NPP data. We would like to thank several of our project staff who have generated the NPP rates in the Indian Ocean that have been utilised for this work. We would like to thank two anonymous reviewers and the Editor-In-Chief, Dr. Javier Aristegui, for their critical review and suggestions to improve the presentation of our results. This has NIO contribution number.....

References:

Barber, R.T., Marra, J., Bidigare, R.C., Codispoti, L.A., Halpern, D., Johnson, Z., Latasa, M., Goericke, R. and Smith, S.L., 2001. Primary productivity and its regulation in the Arabian Sea during 1995. *Deep Sea Research Part II: Topical Studies in Oceanography*, 48(6-7), pp.1127-1172.

- Behrenfeld, M.J. and Falkowski, P.G., 1997. Photosynthetic rates derived from satellite-based chlorophyll concentration. *Limnology and Oceanography*, 42(1), pp.1-20.
- Behrenfeld, M.J., Boss, E., Siegel, D.A. and Shea, D.M., 2005. Carbon-based ocean productivity and phytoplankton physiology from space. *Global biogeochemical cycles*, 19(1).
- Bhattathiri, P.M.A., Pant, A., Sawant, S., Gauns, M., Matondkar, S.G.P., Mohanraju, R. 1996. Phytoplankton production and chlorophyll distribution in the eastern and central Arabian Sea in 1994–1995. *Curr Sci* 71, 857–862.
- Bishop, J. K. B., Calvert, S. E. and Soon, M. Y. S., 1999. Spatial and temporal variability of POC in the northeast Subarctic Pacific, *Deep Sea Research Part II*, 46, 2699–2733.
- Bopp, L., Resplandy, L., Orr, J.C., Doney, S.C., Dunne, J.P., Gehlen, M., Halloran, P., Heinze, C., Ilyina, T., Seferian, R. and Tjiputra, J., 2013. Multiple stressors of ocean ecosystems in the 21st century: projections with CMIP5 models. *Biogeosciences*, 10(10), pp.6225-6245.
- Boyd, P.W., 2015. Toward quantifying the response of the oceans' biological pump to climate change. *Frontiers in Marine Science*, 2, p.77.
- Buitenhuis, E.T., Hashioka, T. and Quéré, C.L., 2013. Combined constraints on global ocean primary production using observations and models. *Global Biogeochemical Cycles*, 27(3), pp.847-858.
- Campbell, J., Antoine, D., Armstrong, R., Arrigo, K., Balch, W., Barber, R., Behrenfeld, M., Bidigare, R., Bishop, J., Carr, M.E., Esaias, W., Falkowski, P., Hoepffner, N., Iverson, R., Kiefer, D., Lohrenz, S., Marra, J., Morel, A., Ryan, J., Vedernikov, V., Waters, K., Yentsch, C., and Yoder, J. 2002. Comparison of algorithms for estimating ocean primary production from surface chlorophyll, temperature and irradiance. *Global Biogeochemical Cycles*, 16(3), doi: 10.1029/2001GB001444.
- Carr, M.E., Friedrichs, M.A., Schmeltz, M., Aita, M.N., Antoine, D., Arrigo, K.R., Asanuma, I., Aumont, O., Barber, R., Behrenfeld, M. and Bidigare, R., 2006. A comparison of global estimates of marine primary production from ocean color. *Deep Sea Research Part II: Topical Studies in Oceanography*, 53(5-7), pp.741-770.
- Chassssignet, E.P., Hurlburt, H.E. Smedstar, O.M. Halliwell, G.R., Hogan, P.J., Wallcraft, A.J., Baraille, R., Bleck, R. 2007. The HYCOM (hybrid coordinate ocean model) data assimilative system. *J. Mar. Syst.*, 65, 60-83.
- Conkright, M.E. Garcia, H.E. O'Brien, T.D., Locarnini, R.A. Boyer, T.P, Stephens, C., and Antonov, J.I. 2002. *World Ocean Atlas 2001*, Vol. 4, Nutrients, edited by S. Levitus, NOAA Atlas NESDID 52, 392 pp. US Gov. Print, Off., Washington D.C.
- Claustre, H., Morel, A., Babin, M., Cailliau, C., Marie, D., Marty, J.-C., Tailliez, D. and Vaultot, D. 1999. Variability in particle attenuation and chlorophyll fluorescence in the tropical Pacific: Scales, patterns, and biogeochemical implications, *Journal of Geophysical Research*, 104, 3401–3422.
- D'Mello, J.R. and Prasanna Kumar, S., 2018. Processes controlling the accelerated warming of the Arabian Sea. *International Journal of Climatology*, 38(2), pp.1074-1086.

- Dalabehara, H.B. and Sarma, V.V.S.S., 2021. Physical forcing controls spatial variability in primary production in the Indian Ocean. *Deep Sea Research Part II: Topical Studies in Oceanography*, 183, p.104906.
- De Sousa, S. N., Kumar, M. D., Sardessai, S., Sarma, V. V. S. S., and Shirodkar, P. V. 1996. Seasonal variability in oxygen and nutrients in the central and eastern Arabian Sea, *Curr. Sci.*, 71: 847–851.
- Eppley, R.W., 1972. Temperature and phytoplankton growth in the sea. *Fishery bulletin*, 70(4), 1063-1085.
- Field, C.B., Behrenfeld, M.J., Randerson, J.T. and Falkowski, P., 1998. Primary production of the biosphere: integrating terrestrial and oceanic components. *science*, 281(5374), pp.237-240.
- Gauns, M., Madhupratap, M., Ramaiah, N., Jyothibabu, R., Fernandes, V., Paul, J.T., Prasanna Kumar, S., 2005. Comparative accounts of biological productivity characteristics and estimates of carbon fluxes in the Arabian Sea and Bay of Bengal. *Deep-Sea Res., II* 52, 2003-2017.
- Geider, R. J., 1987. Light and temperature dependence of the carbon to chlorophyll ratio in microalgae and cyanobacteria: Implications for physiology and growth of phytoplankton, *New Phytology*, 106, 1–34.
- Gomes, H.R., Goes, J.I., Saino, T., 2000. Influence of physical process and freshwater discharge on the seasonality of phytoplankton regime in the Bay of Bengal. *Cont. Shelf Res.*, 20, 313–330.
- Gregg, W.W. and Rousseaux, C.S., 2019. Global ocean primary production trends in the modern ocean color satellite record (1998–2015). *Environmental Research Letters*, 14(12), p.124011.
- Gruber, N., Gloor, M., Mikaloff Fletcher, S.E., Doney, S.C., Dutkiewicz, S., Follows, M.J., Gerber, M., Jacobson, A.R., Joos, F., Lindsay, K. and Menemenlis, D., 2009. Oceanic sources, sinks, and transport of atmospheric CO₂. *Global biogeochemical cycles*, 23(1).
- Henson, S.A., Sanders, R., Madsen, E., Morris, P.J., Le Moigne, F. and Quartly, G.D., 2011. A reduced estimate of the strength of the ocean's biological carbon pump. *Geophysical Research Letters*, 38(4).
- Kurian, S., Shenoy, D.M., Akhi, V.P., Kessarkar, P.M., Gauns, M., Shetye, S.S., Kabeer, M., Vijayan, A.P., Methar, A., Karapurkar, S., Chandrasekhararao, A.V., Naqvi, S.W.A., 2023. Spatial and seasonal variations in the particulate sinking flux in the Bay of Bengal. *Progress in Oceanography*, 211, 102983.
- Longhurst, A., Sathyendranath, S., Platt, T. and Caverhill, C., 1995. An estimate of global primary production in the ocean from satellite radiometer data. *Journal of plankton Research*, 17(6), pp.1245-1271.
- Löscher, C.R., 2021. Reviews and syntheses: Trends in primary production in the Bay of Bengal—is it at a tipping point?. *Biogeosciences*, 18(17), pp.4953-4963.
- Lurin, B., 1994. Global terrestrial net primary production. *Glob. Change News I.(IGPB)*, 19, pp.6-8.

MacIntyre, H. L., Kana, T. M., Anning, T. and Geider, R. J., 2002. Photoacclimation of photosynthesis irradiance response curves and photosynthetic pigments in microalgae and cyanobacteria, *Journal of Phycology*, 38, 17–38.

Madhupratap, M., Kumar, S.P., Bhattathiri, P. M. A., Kumar, M.D., Raghukumar, S., Nair, K. K. C. and Ramaiah, N. . 1996. Mechanism of the biological response to winter cooling in the northeastern Arabian Sea, *Nature*, 384: 549–552, 1996.

Maneesha, K., Sarma, V.V.S.S., Reddy, N.P.C., Sadhuram, Y., Murty, T.R., Sarma, V.V. and Kumar, M.D., 2011. Meso-scale atmospheric events promote phytoplankton blooms in the coastal Bay of Bengal. *Journal of earth system science*, 120, pp.773-782.

Mikaloff Fletcher, S.E., Gruber, N., Jacobson, A.R., Gloor, M., Doney, S.C., Dutkiewicz, S., Gerber, M., Follows, M., Joos, F., Lindsay, K. and Menemenlis, D., 2007. Inverse estimates of the oceanic sources and sinks of natural CO₂ and the implied oceanic carbon transport. *Global Biogeochemical Cycles*, 21(1).

Murtugudde, R. and Busalacchi, A.J., 1999. Interannual variability of the dynamics and thermodynamics of the tropical Indian Ocean. *Journal of Climate*, 12(8), pp.2300-2326.

Modi, A. and Roxy, M.K., 2023. Past Trends and Future Projections of Marine Primary Productivity in the Tropical Indian Ocean. In *Dynamics of Planktonic Primary Productivity in the Indian Ocean* (pp. 191-206). Cham: Springer International Publishing.

Morel, A., and Ahn, Y.-H., 1991. Optics of heterotrophic nanoflagellates and ciliates: A tentative assessment of their scattering role in oceanic waters compared to those of bacterial and algal cells, *Journal of Marine Research*, 48, 1 – 26.

Morrison, J. M., Codispoti, L., Gaurin, S., Jones, B., Manghnani, V., and Zheng, Z. 1998. Seasonal variation of hydrographic and nutrient fields during the US JGOFS Arabian Sea Process Study, *Deep Sea Res., Part II*, 45: 2053–2101.

Prasanna Kumar, S., Nuncio, M., Narvekar, J., Kumar, A., Sardesai, D.S., De Souza, S.N., Gauns, M., Ramaiah, N. and Madhupratap, M., 2004. Are eddies nature's trigger to enhance biological productivity in the Bay of Bengal?. *Geophysical Research Letters*, 31(7).

Qasim S.Z., 1977. Biological productivity of the Indian Ocean. *Indian Journal of Marine Science*, 6, 122-137.

Qasim, S.Z., 1982. Oceanography of the northern Arabian Sea. *Deep-Sea Research*, 29, 1041-1068.

Ramaiah, N., Fernandes, V., Paul, J.T., Jyothibabu, R., Mangesh, G. and Jayraj, E.A., 2010. Seasonal variability in biological carbon biomass standing stocks and production in the surface layers of the Bay of Bengal.

Rao, D.N. and Sarma, V.V.S.S., 2022. Accumulation of dissolved organic carbon and nitrogen in the photic zone in the nitrogen-depleted waters of the Bay of Bengal. *Marine Chemistry*, 239, p.104074.

Reagan, J.R., Seidov, D., Wang, Z., Dukhovskoy, D., Boyer, T.P., Locarnini, R.A. and Baranova, O.K., 2024. *World Ocean Atlas 2023, Volume 2: Salinity*. A. Mishonov, Tech. Ed. NOAA Atlas NESDIS, 90, p.51pp.

- Roxy, M.K., Modi, A., Murtugudde, R., Valsala, V., Panickal, S., Prasanna Kumar, S., Ravichandran, M., Vichi, M. and Lévy, M., 2016. A reduction in marine primary productivity is driven by rapid warming over the tropical Indian Ocean. *Geophysical Research Letters*, 43(2), pp.826-833.
- Roxy, M.K., Ritika, K., Terray, P., Murtugudde, R., Ashok, K. and Goswami, B.N., 2015. Drying of the Indian subcontinent by rapid Indian Ocean warming and a weakening land-sea thermal gradient. *Nature communications*, 6(1), p.7423.
- Sakshaug, E., Andresen, K. and Kiefer, D. A., 1989. A steady state description of growth and light absorption in the marine planktonic diatom *Skeletonema costatum*, *Limnology and Oceanography*, 34, 198–205.
- Sarma, V.V.S.S., Yadav, K., and Behera, S. 2019. Role of eddies on organic matter production and f-ratios in the Bay of Bengal. *Marine Chemistry*, 210, 13-23.
- Sarma, V.V.S.S. and Dalabehera, H.B., 2019. New and primary production in the western Indian Ocean during fall monsoon. *Marine Chemistry*, 215, p.103687.
- Sarma, V.V.S.S., Krishna, M.S., Viswanadham, R., Rao, G.D., Rao, V.D., Sridevi, B., Kumar, B.S.K., Prasad, V.R., Subbaiah, C.V., Acharyya, T. and Bandopadhyay, D., 2013. Intensified oxygen minimum zone on the western shelf of Bay of Bengal during summer monsoon: influence of river discharge. *Journal of Oceanography*, 69, pp.45-55.
- Sarma, V.V.S.S., Jagadeesan, L., Dalabehera, H.B., Rao, D.N., Kumar, G.S., Durgadevi, D.S., Yadav, K., Behera, S. and Priya, M.M.R., 2018. Role of eddies on the intensity of oxygen minimum zone in the Bay of Bengal. *Continental Shelf Research*, 168, pp.48-53.
- Sarma, V.V.S.S., Prasad, M.H.K. and Dalabehera, H.B., 2021. Influence of phytoplankton pigment composition and primary production on pCO₂ levels in the Indian Ocean. *Journal of Earth System Science*, 130(2), p.85.
- Sarma, V.V.S.S., Sridevi, B., Kumar, A., Bikkina, S., Kumari, V.R., Bikkina, P., Yadav, K. and Rao, V.D., 2022. Impact of atmospheric anthropogenic nitrogen on new production in the northern Indian Ocean: constrained based on satellite aerosol optical depth and particulate nitrogen levels. *Environmental Science: Processes & Impacts*, 24(10), pp.1895-1911.
- Sarma, V.V.S.S., Sridevi, B., Metzl, N., Patra, P.K., Lachkar, Z., Chakraborty, K., Goyet, C., Lévy, M., Mehari, M. and Chandra, N., 2023. Air-Sea fluxes of CO₂ in the Indian Ocean between 1985 and 2018: A synthesis based on Observation-based surface CO₂, hindcast and atmospheric inversion models. *Global Biogeochemical Cycles*, 37(5), p.e2023GB007694.
- Satya Prakash, S.P., Ramesh, R., Sheshshayee, M.S., Rahul Mohan, R.M. and Sudhakar, M., 2015. Nitrogen uptake rates and f-ratios in the Equatorial and Southern Indian Ocean. *Current Science*, pp.239-245
- Schott, F.A., Xie, S.P. and McCreary Jr, J.P., 2009. Indian Ocean circulation and climate variability. *Reviews of Geophysics*, 47(1).
- Sherin, C.K., Sarma, V.V.S.S., Rao, G.D., Viswanadham, R., Omand, M.M., Murty, V.S.N. 2018. New to total primary production ratio (f-ratio) in the Bay of Bengal using isotopic composition of suspended particulate organic carbon and nitrogen. *Deep-Sea Research, Part I*, 139, 43-54.

Silsbe, G.M., Behrenfeld, M.J., Halsey, K.H., Milligan, A.J. and Westberry, T.K., 2016. The CAFÉ model: A net production model for global ocean phytoplankton. *Global Biogeochemical Cycles*, 30(12), pp.1756-1777.

Sridevi, B., Sabira, S. and Sarma, V.V.S.S., 2023. Impact of ocean warming on net primary production in the northern Indian Ocean: role of aerosols and freshening of surface ocean. *Environmental Science and Pollution Research*, 30(18), pp.53616-53634.

Tagliabue, A., Kwiatkowski, L., Bopp, L., Butenschön, M., Cheung, W., Lengaigne, M. and Vialard, J., 2021. Persistent uncertainties in ocean net primary production climate change projections at regional scales raise challenges for assessing impacts on ecosystem services. *Frontiers in Climate*, 3, <https://doi.org/10.3389/fclim.2021.738224>

Tandule, C.R., Gogoi, M.M., Kotalo, R.G. and Babu, S.S., 2022. On the net primary productivity over the Arabian Sea due to the reduction in mineral dust deposition. *Scientific Reports*, 12(1), p.7761.

Westberry, T., Behrenfeld, M.J., Siegel, D.A. and Boss, E., 2008. Carbon-based primary productivity modelling with vertically resolved photoacclimation. *Global Biogeochemical Cycles*, 22(2).

Xie, S.P., Annamalai, H., Schott, F.A. and McCreary, J.P., 2002. Structure and mechanisms of South Indian Ocean climate variability. *Journal of Climate*, 15(8), pp.864-878.

Table 1: Details of the data used for comparison, including period of collection, region, number of stations and tracer used for NPP measurements and source of data are given.

| Cruise name | Period of sampling | Area of Sampling | No of stations measured | Tracer used | Reference |
|-------------|------------------------|-----------------------------|-------------------------|-----------------|------------------------------|
| SS190 | December-2000 | Northeast AS | 6 | ¹⁴ C | Balachandran et.al., 2008 |
| SS198 | December-2001 | Northwest BoB | 6 | ¹⁴ C | Balachandran et.al., 2008 |
| ML-LRAP | April 2001 | Western BoB | 12 | ¹⁴ C | Madhu et al., 2006 |
| ML-LRAP | July 2001 | Western BoB | 12 | ¹⁴ C | Madhu et al., 2006 |
| ML-LRAP | December 2001 | Western BoB | 12 | ¹⁴ C | Madhu et al., 2006 |
| SK182 | September-October 2002 | Central and Eastern BoB | 18 | ¹⁴ C | Gauns et al., 2005 |
| SS244 | April 2009 | Eastern AS | 7 | ¹³ C | Gandhi et al., 2010 |
| ABP35 | February – April 2009 | SIO | 11 | ¹³ C | Gandhi et al., 2012 |
| SN | Feb 2010 | SIO | 6 | ¹⁴ C | Tripathy et al., 2014 |
| SK304 | April 2013 | Central BoB | 12 | ¹³ C | Anand et al., 2024 submitted |
| SSK60 | January 2014 | Central AS | 20 | ¹³ C | Sarma et al., 2018 |
| SK311 | April 2014 | Central Indian Ocean | 25 | ¹³ C | Dalabehera and Sarma, 2021 |
| SN | June 2014 | SIO | 7 | ¹⁴ C | Tripathy et al., 2020 |
| SSK77 | February 2015 | Central AS | 9 | ¹³ C | Unpublished |
| SSD01 | August 2015 | Central BoB and Andaman Sea | 14 | ¹³ C | Unpublished |
| SK324 | October 2015 | AS and SIO | 20 | ¹³ C | Sarma and Dalabehera, 2019 |
| Shiyan3 | February-April 2017 | Central BoB and eastern SIO | 14 | ¹⁴ C | Liu et al., 2021 |
| SSK118 | March-April 2018 | Western and Central BoB | 9 | ¹³ C | Sarma et al., 2019 |
| SN132 | July-August 2018 | Central BoB | 8 | ¹³ C | Saxena et al., 2020 |
| SN142 | June 2019 | Western and Central BoB | 13 | ¹³ C | Rao and Sarma 2021 |
| SSK144 | September 2022 | Western and Central BoB | 15 | ¹³ C | Unpublished |

ABP=Akademik Boris Petrov; SSK-Sindhu Sankalp; SSD=Sindhu Sadhana; SK=Sagar Kanya; SN=Sagar Nidhi

Table 2: Different parameters used in various NPP models. X indicates used parameter in the model

| Parameter | VGPM | CbPM | Eppley-VGPM | CAFE | OC-CCI |
|------------|------|------|-------------|------|--------|
| SST | X | | X | X | |
| Chl-a | X | X | X | X | X |
| PAR | X | X | X | X | X |
| b_{bp} | | X | | X | X |
| a_{ph} | | | | X | X |
| a_{dg} | | | | X | X |
| K_d | | X | | X | X |
| η | | | | X | |
| b_{bw} | | | | X | X |
| MLD | | X | | X | |
| Nitracline | | X | | | |
| SSS | | | | X | |

Table 3: Performance indices for the relative errors between measured and different model-derived NPP in different sub-basins of the Indian Ocean.

| Indices | VGPM | CbPM | Eppley-VGPM | CAFE |
|---------------------------|-------|--------|-------------|--------|
| Arabian Sea | | | | |
| N | 27 | 27 | 27 | 27 |
| Slope | 0.40 | 1.40 | 1.01 | -0.34 |
| Intercept | 188.4 | -67.9 | 293.4 | 733.1 |
| R | 0.53 | 0.86 | -0.55 | -0.58 |
| R ² | 0.28 | 0.74 | 0.30 | 0.34 |
| r | 1.54 | 0.81 | 0.75 | 1.63 |
| LogRMSE | 0.05 | 0.02 | 0.05 | 0.07 |
| UPD (%) | 36.9 | -22.9 | -32.9 | 28.9 |
| M | 0.17 | -0.10 | -0.15 | 0.11 |
| S | 0.15 | 0.10 | 0.17 | 0.24 |
| Fmin | 1.03 | 0.63 | 0.48 | 0.74 |
| Fmed | 1.46 | 0.89 | 0.71 | 1.39 |
| Fmax | 41.38 | 7.82 | 7.45 | 33.93 |
| Bay of Bengal | | | | |
| N | 89 | 89 | 89 | 89 |
| Slope | 0.77 | 1.30 | 1.59 | -0.02 |
| Intercept | 112.3 | 226.5 | 195.0 | 478.6 |
| R | 0.73 | 0.65 | 0.72 | -0.02 |
| R ² | 0.54 | 0.42 | 0.52 | 0.00 |
| r | 0.96 | 0.55 | 0.48 | 0.87 |
| LogRMSE | 0.01 | 0.10 | 0.12 | 0.06 |
| UPD (%) | -7.80 | -60.76 | -71.49 | -27.79 |
| M | -0.03 | -0.28 | -0.33 | -0.12 |
| S | 0.12 | 0.14 | 0.12 | 0.21 |
| Fmin | 0.71 | 0.38 | 0.35 | 0.47 |
| Fmed | 0.92 | 1.53 | 1.47 | 0.75 |
| Fmax | 10.98 | 4.67 | 3.86 | 9.07 |
| South Indian Ocean | | | | |
| N | 62 | 62 | 62 | 62 |
| Slope | 0.28 | 0.27 | 0.45 | 0.35 |
| Intercept | 171.8 | 261.78 | 149.1 | 306.0 |
| R | 0.28 | 0.34 | 0.57 | 0.61 |
| R ² | 0.08 | 0.24 | 0.32 | 0.38 |
| r | 1.68 | 1.14 | 1.34 | 0.83 |
| LogRMSE | 0.10 | 0.07 | 0.06 | 0.05 |
| UPD (%) | 29.29 | -2.65 | 15.91 | -25.49 |
| M | 0.14 | -0.01 | 0.07 | -0.12 |
| S | 0.29 | 0.26 | 0.23 | 0.19 |
| Fmin | 0.71 | 0.54 | 0.70 | 0.49 |
| Fmed | 1.38 | 0.90 | 1.18 | 0.76 |
| Fmax | 46.34 | 16.78 | 25.68 | 8.98 |

Legend to figures

Figure 1: The number of NPP observations carried out during each month in the a) Arabian Sea, b) BoB, and c) SIO.

Figure 2: a) The mean measured photic zone integrated Chl-a (mg m^{-2}) (b), the mean photic zone integrated Primary production ($\text{mgC m}^{-2} \text{d}^{-1}$) and (c) photic zone mean PB ($\text{mgC mgChl-a}^{-1} \text{d}^{-1}$) in different regions of the Indian Ocean. The variability in the data is shown as standard deviation.

Figure 3: a) The NPP measured between 2003 and 2022 in the Indian Ocean and the estimated NPP by b) VGPM, c) CbPM, d) Eppley-VGPM, and e) CAFE models at the same location of measured NPP are given in $\text{mgC m}^{-2} \text{d}^{-1}$.

Figure 4: The spatial variability in annual mean NPP in the Indian Ocean by a) VGPM, b) CbPM, c) Eppley-VGPM, and d) CAFE ($\text{mgC m}^{-2} \text{d}^{-1}$) models.

Figure 5: Comparison of annual and basin mean measured and modelled NPP in a) the Arabian Sea, b) the BoB, and c) the SIO. The variations in the data with reference to space and time are given as standard deviations.

Figure 6: The monthly basin mean NPP by different models and measured NPP in the a) Arabian Sea, b) BoB, and c) SIO is shown. The standard deviations in each basin is given. The mean measured NPP values are given in black line graph.

Figure 7: The spatial variations in trends in NPP during different seasons, winter (December to February), spring (March to May), summer (June to September), and fall (October to November) by different models are given. The significance at 90% is given in a black line. Blue and red colours indicate declining and increasing trends, respectively.

Figure 1:

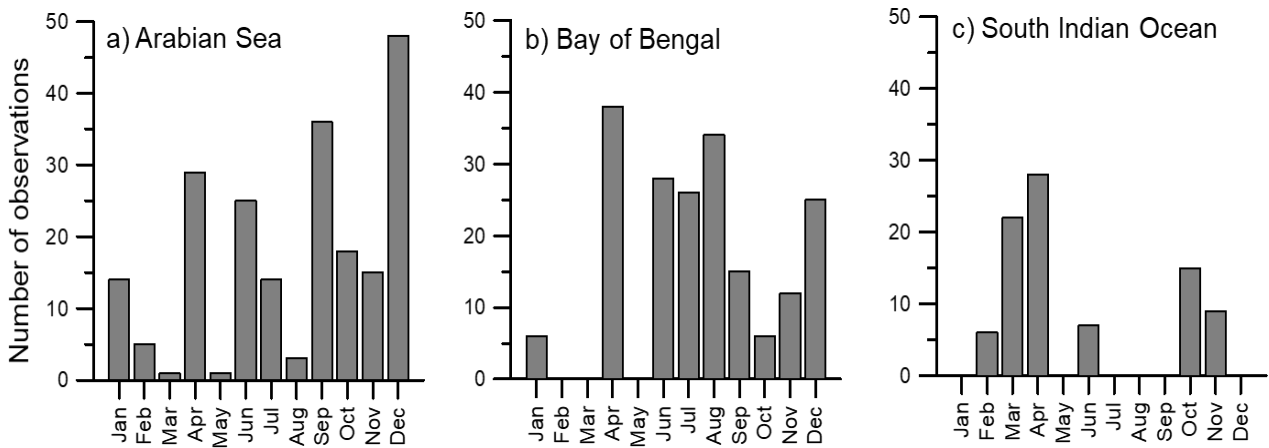


Figure 2:

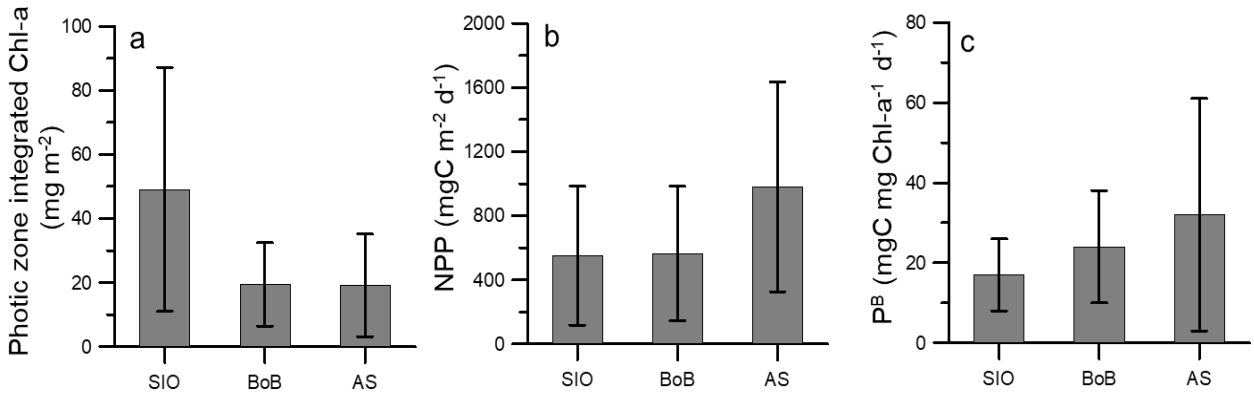


Figure 3:

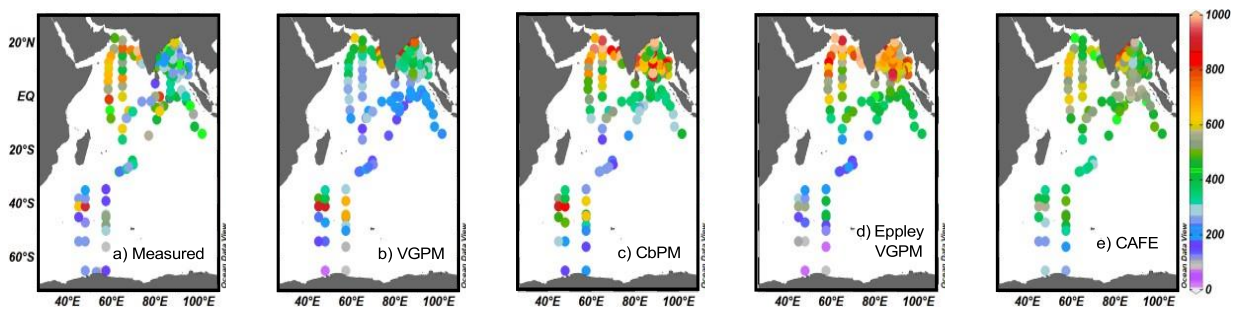


Figure 4:

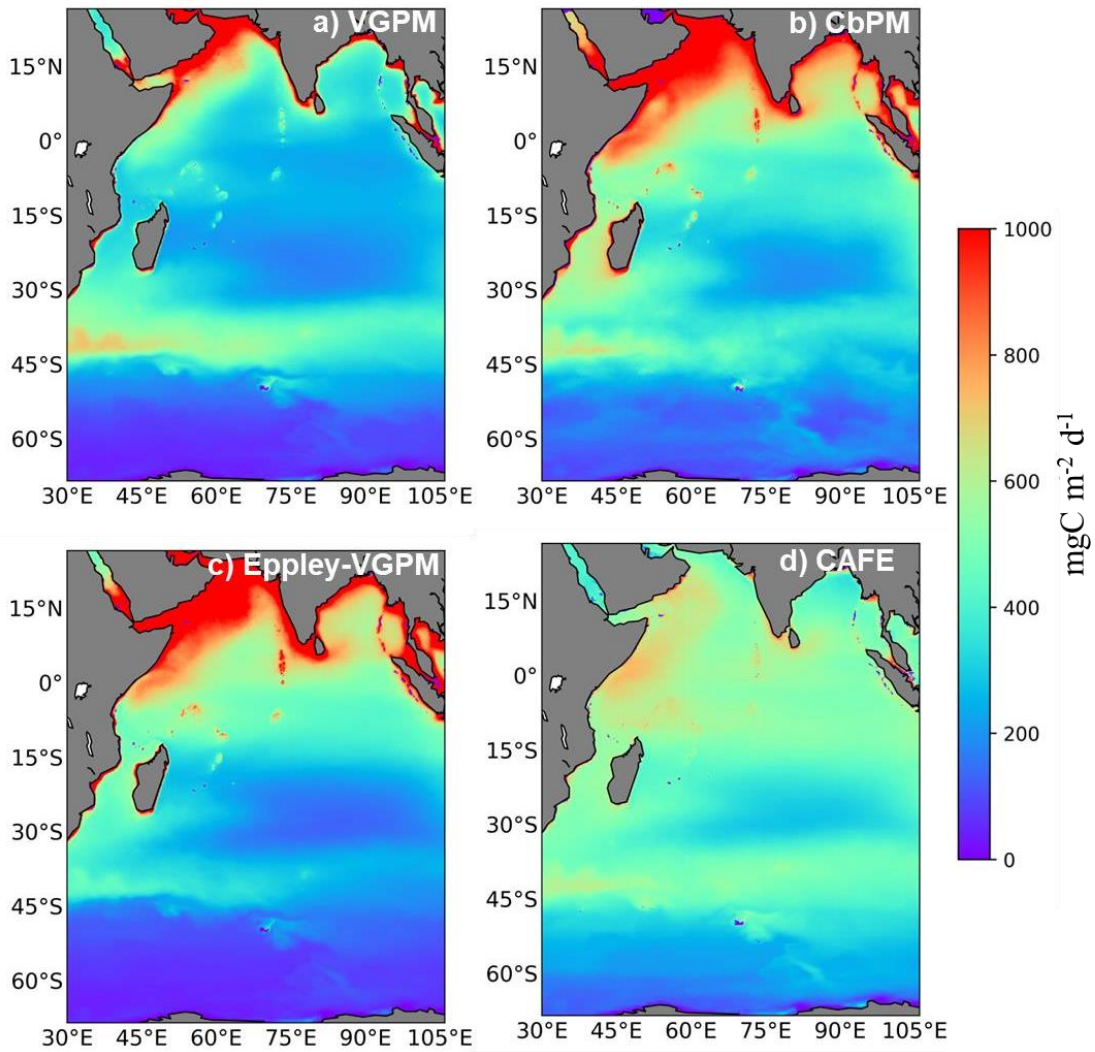


Figure 5:

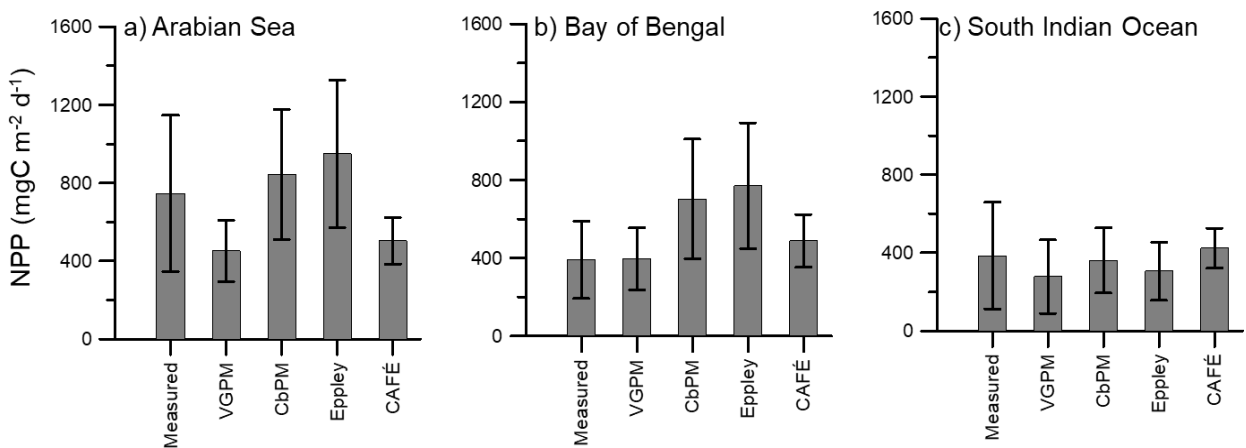


Figure 6:

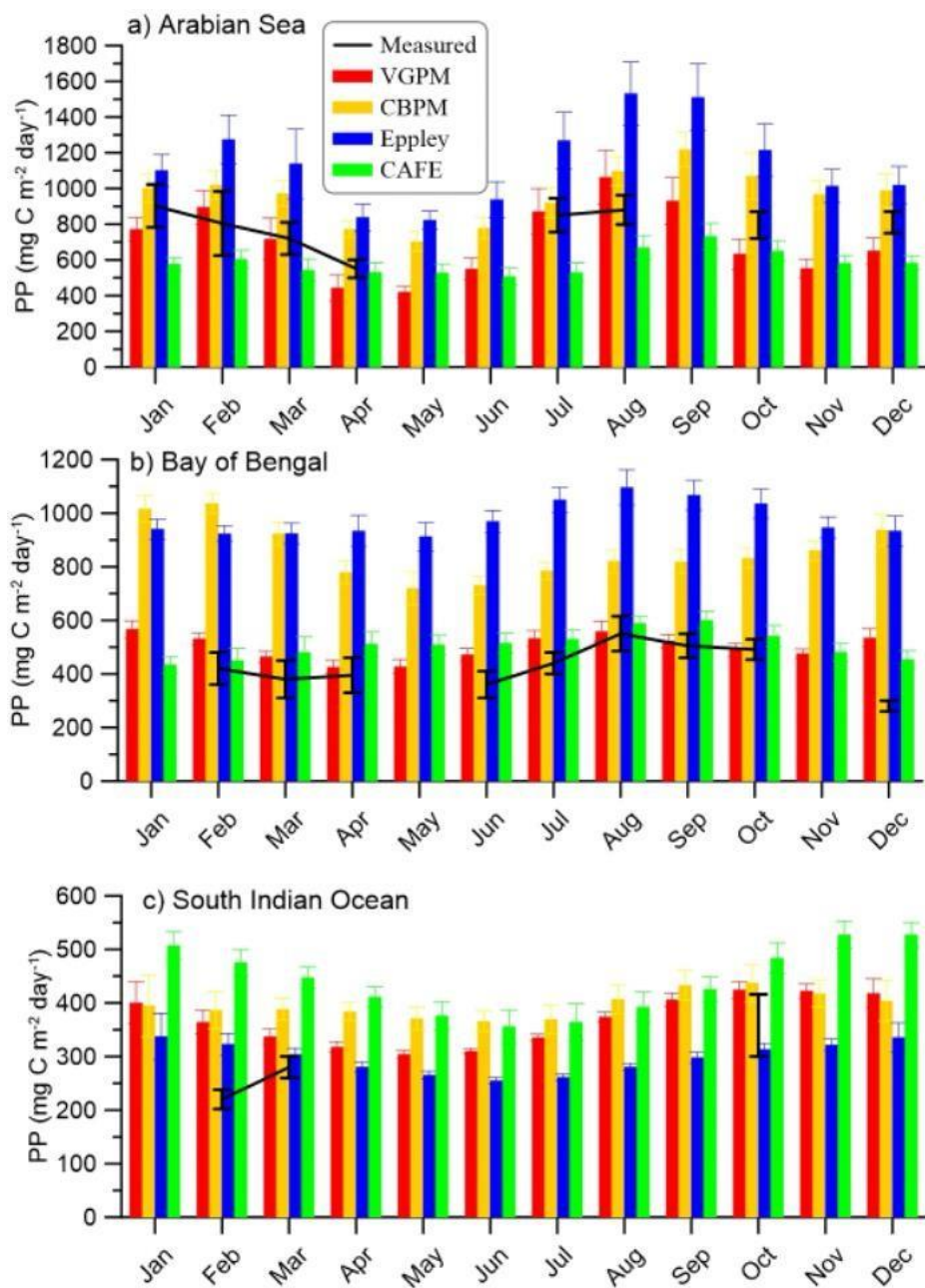
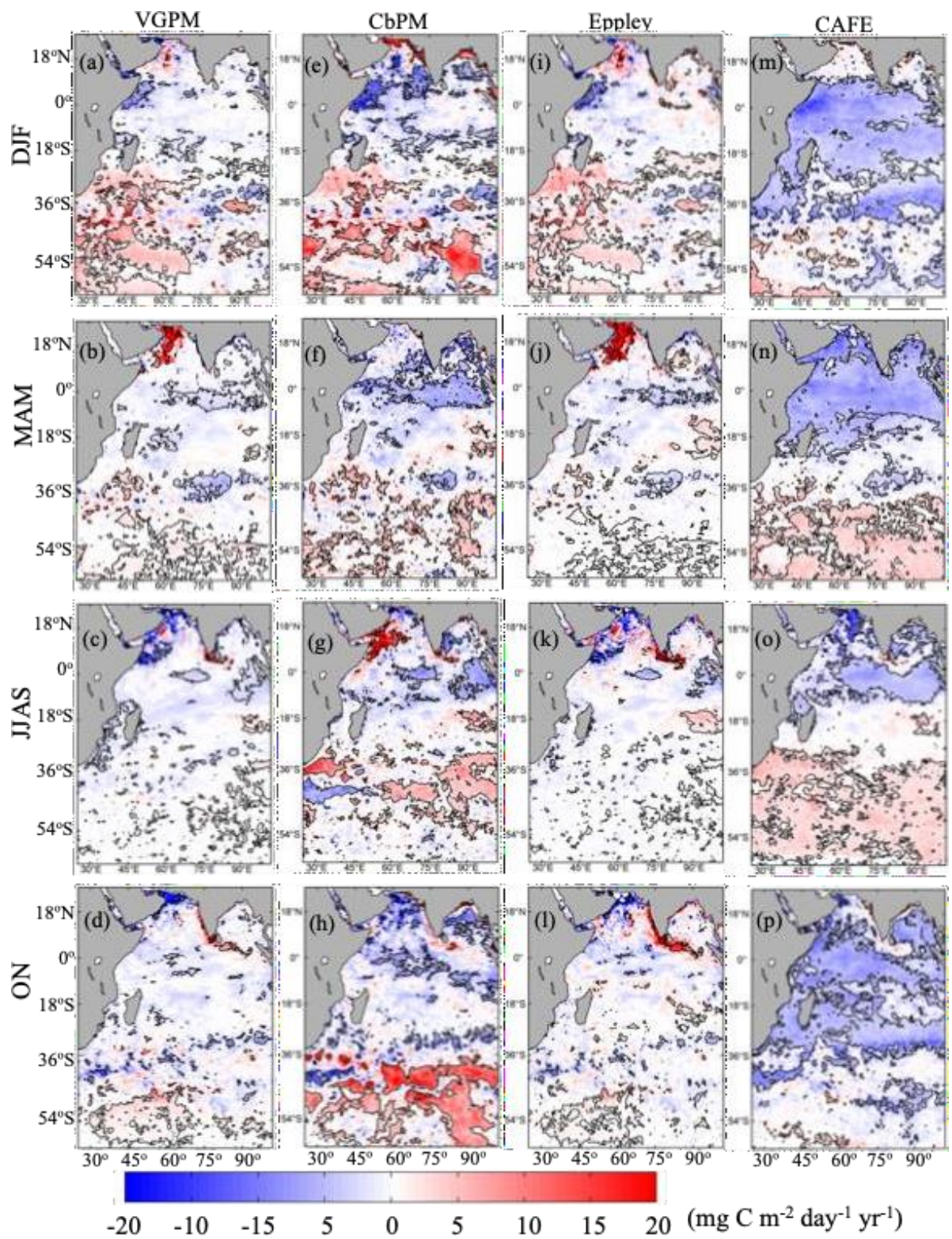


Figure 7:



Supplementary Figure S1: The monthly mean climatological nitrate ($\mu\text{mol kg}^{-1}$) concentrations in the surface waters in the northern Indian Ocean (Reagon et al., 2024)

